PHILOSOPHICAL TRANSACTIONS OF THE ROYAL SOCIETY A MATHEMATICAL, PHYSICAL & ENGINEERING SCIENCES

Solitary-Like Waves in Boundary-Layer Flows and their Randomization

E. V. Bogdanova-Ryzhova and O. S. Ryzhov

Phil. Trans. R. Soc. Lond. A 1995 **352**, 389-404
doi: 10.1098/rsta.1995.0078

Solitary-like waves in boundary-layer flows and their randomization

By E. V. Bogdanova-Ryzhova and O. S. Ryzhov

Department of Mathematical Sciences, Rensselaer Polytechnic Institute, Troy, NY 12180-3590, USA

Essentially nonlinear motions generated in incompressible boundary layers by external agencies are considered. A pertinent mathematical model for the Blasius flow is furnished by the forced Benjamin–Davis–Acrivos integral–differential equation. A steady hump is chosen as a simplest source in order to trace the disturbance-pattern evolution as the roughness height increases, provided that its length is kept fixed. Occurence of bifurcation phenomena features this problem; the first publication gives rise, in particular, to a specific regime with nearly limit-cycle-type oscillations in the immediate vicinity of the hump. After the second bifurcation studied, the nearly periodic regime collapses into irregular pulsations with erratic sequences of amplitudes and characteristic times. A brief discussion based on the forced Korteweg–de Vries equation lends credence to the view that the chaotically transitional process can be triggered at an earlier stage of wave amplification.

1. Introduction

Nonlinear stages of the Tollmien–Schlichting (TS) wave development, in incompressible boundary layers of different kinds, play a key role in understanding the mechanisms behind the onset of random elements in fluid motion before laminar/turbulent transition. The first stage sets in very rapidly and is governed by the weakly nonlinear theory – the basic concepts of which have been advanced in general terms by Landau (see, for example, Landau & Lifshitz 1944) and, as applied to shear flows, worked out in great depth by Stuart (1960). The resonant-triad interaction (Craik 1971) is an extension of this theory to three-dimensional disturbances giving rise to the N-route to transition, observed by Kachanov *et al.* (1977) in wind-tunnel tests. A more sophisticated consideration of N-breakdown, with references to many original results, ensuing, in particular, from the Floquet approach, is available in Kachanov *et al.* (1993). However, it seems likely that essentially nonlinear properties of the disturbance-amplification process may come first whilst a strong 'three dimensionalization' of the velocity field begins to manifest itself at some position further downstream if an initial weak TS harmonic wave train is artificially excited in a boundary layer under carefully controlled conditions (Kachanov *et al.* 1989). Thus, a two-dimensional oscillation pattern yields not only the simplest mathematical model of the second truly nonlinear stage but is closely related to experimental findings as well (Kachanov *et al.* 1993). The further build-up of the wave amplitude in these circumstances terminates in the K-route to transition, discovered by Klebanoff (see, for example, Klebanoff *et al.* 1962).

Phil. Trans. R. Soc. Lond. A (1995) **352**, 389–404
Printed in Great Britain

Theoretically, the second stage has been independently analysed by Zhuk & Ryzhov (1982) and Smith & Burggraf (1985) on the assumption that the non-dimensional pressure variations range up to $O(\Delta^2)$, $\varepsilon = Re^{-1/8} \ll \Delta \ll 1$ and the velocity field remains two dimensional when the Reynolds number Re tends to infinity. Then, upon introducing appropriately scaled variables, the problem is reduced to a system of equations,

$$\frac{\partial u}{\partial x} + \frac{\partial v}{\partial y} = 0, \quad \frac{\partial u}{\partial t} + u\frac{\partial u}{\partial x} + v\frac{\partial u}{\partial y} = -\frac{\partial p}{\partial x}, \quad \frac{\partial p}{\partial y} = 0, \tag{1.1}$$

controlling, to leading order, the disturbance pattern within a thin adjustment sublayer. Here t is the time; x, y designate the Cartesian coordinates with x being aligned with the direction of an oncoming stream; u, v are the velocity components; and p denotes the excess pressure. The limiting conditions, as the normal coordinate $y \to \infty$, read

$$u - \tilde{A} \to y, \quad v + \frac{\partial \tilde{A}}{\partial x} y \to -\frac{\partial \tilde{A}}{\partial t} - \tilde{A}\frac{\partial \tilde{A}}{\partial x} - \frac{\partial p}{\partial x}. \tag{1.2}$$

For an incompressible Blasius boundary layer, the self-induced pressure entering (1.1), (1.2) is related to the unknown instantaneous displacement thickness $A = -\tilde{A}$ through

$$p(t,x) = \frac{1}{\pi}\int_{-\infty}^{\infty} \frac{\partial \tilde{A}/\partial X}{x - X}(t, X)\,\mathrm{d}X. \tag{1.3}$$

It is easy to verify that the limiting conditions (1.2) provide an exact solution to (1.1), regardless of the dependence of p on $\tilde{A}$. Thus, what still remains to be done, if we confine ourselves to analysing free oscillations in the adjustment sublayer on a flat plate, is to meet the slip condition $v = 0$ at $y = 0$. Then, substituting (1.3) for p results in the Benjamin–Davis–Acrivos (BDA) integral-differential equation

$$\frac{\partial \tilde{A}}{\partial t} + \tilde{A}\frac{\partial \tilde{A}}{\partial x} = \frac{1}{\pi}\int_{-\infty}^{\infty} \frac{\partial^2 \tilde{A}/\partial X^2}{X - x}\,\mathrm{d}X \tag{1.4}$$

determining the displacement-thickness evolution in time and distance along the solid surface. This famous equation derives its name from Benjamin (1967) and Davis & Acrivos (1967). The BDA equation was applied in Kachanov *et al.* (1993) to shed new light upon the appearance of sharp narrow spikes, on the velocity oscilloscope traces, which are characteristic of the K-route to breakdown. An explanation for the spikes in terms of BDA-soliton properties, which proved to be in close agreement with the results of wind-tunnel tests, lent credence to the suitability of (1.4) for studying bursting phenomena before the onset of transition.

Let us turn to an essentially nonlinear receptivity problem assuming again that the pressure-oscillation amplitude amounts to as high as $O(\Delta^2)$. In this range of disturbance sizes, (1.1) hold true, whereas (1.2) yield a solution which automatically satisfies the limiting conditions at the upper reaches of the adjustment sublayer as $y \to \infty$. The wave motion is supposed to be excited by a local roughness $y = y_{\mathrm{w}}(t, x)$, $-b \leqslant x \leqslant b$ on an otherwise flat plate $y = 0$. Then, instead of $v = 0$ at $y = 0$, a constraint

$$v = \frac{\partial y_{\mathrm{w}}}{\partial t} + u\frac{\partial y_{\mathrm{w}}}{\partial x} \tag{1.5}$$

is met at the rough surface. Substituting (1.2) and (1.3) into (1.5) and replacing the

displacement thickness by $A = -\tilde{A} = y_w + \tilde{A}_w$, we arrive at the inhomogeneous BDA equation

$$\frac{\partial A_w}{\partial t} + A_w \frac{\partial A_w}{\partial x} = \frac{1}{\pi} \int_{-\infty}^{\infty} \frac{\partial^2 A_w / \partial x^2}{X - x} \, dX - f, \tag{1.6}$$

$$f = \frac{1}{\pi} \int_{-\infty}^{\infty} \frac{\partial^2 y_w / \partial X^2}{X - x} \, dX. \tag{1.7}$$

Here the forcing term $f(t, x)$ discloses the mechanism through which the disturbance emission is driven by changes occuring in the surface shape. With $y_w = 0$, $A = -A_w$, and (1.4) is retrieved. In what follows, the roughness is regarded to be a hump; in this case, two bifurcations, accompanied by the appearance of erratic elements in fluid motion, feature the wave-generation process. Oscillations excited by dents exhibit similar distributions in space when the forcing amplitude is varying; for that reason they are left beyond the present discussion.

The forced BDA equation in the form of equation (1.6), as well as the forced KdV equation, have been used primarily in describing waves emitted and sustained at nearly resonant conditions, with applications to atmospheric (lee disturbances behind a mountain ridge) and oceanic (tidal flows over sills) phenomena. The recent papers by Grimshaw & Smyth (1986), Camassa & Wu (1991*a*, *b*) and Mitsudera & Grimshaw (1991) give an idea of the state of the art in this field, whereas comparisons between some theoretical predictions and experimental data are available in Lee *et al.* (1989). However, it is worth keeping in mind that the forcing term controlling the atmospheric and oceanic wave generation is defined in a different way than in (1.7).

2. General statements

We begin by discussing some properties inherent in the forced BDA equation which come as simple extensions of the corresponding propositions known for the homogeneous equation.

Property 1. Let the forcing term on the right-hand side of (1.6) be $f = \partial P / \partial x$, where a periodic function

$$P = \frac{a_1}{1 - \Delta \cos \xi} - \frac{a_2}{2(1 - \Delta \cos \xi)^2}, \quad \xi = kx - \omega t \tag{2.1}$$

depends on five arbitrary constants ω, k, a_1, a_2 and Δ. There then exists a periodic solution

$$A_w = b_1 - \frac{b_2}{1 - \Delta \cos \xi} \tag{2.2}$$

with coefficients b_1 and b_2 given by

$$b_1 = \frac{1}{k} \left[\omega + \frac{k^2}{(1 - \Delta^2)^{1/2}} \right] + \frac{a_1}{b_2}, \quad b_2 = k(1 - \Delta^2)^{1/2} \left\{ 1 + \left[1 + \frac{a_2}{k^2 (1 - \Delta^2)} \right]^{1/2} \right\}. \tag{2.3}$$

If $a_1 = a_2 = 0$ in (2.1), i.e. the forcing agency becomes zero, we find from (2.3) the same values of b_1 and b_2 as those entering a solution to the homogeneous equation (Benjamin 1967).

Property 2. An algebraic solitary-wave-type solution can be derived by passing, in (2.1)–(2.3), to a limit as $k \to 0$, $\Delta \to 1$ with

$$\frac{\omega}{k} = c, \quad \frac{(1-\Delta^2)^{1/2}}{k} = c_0, \quad \frac{a_1}{k^2} = \frac{c_1}{2}, \quad \frac{a_2}{k^2(1-\Delta^2)} = c_2$$

preserved invariant. The final result is cast in the form

$$P = \frac{c_1}{c_0^2 + (x-ct)^2} - \frac{2c_0^2 c_2}{[c_0^2 + (x-ct)^2]^2}, \tag{2.4}$$

$$A_{\mathrm{w}} = c + c_0^{-1} + \frac{c_1}{2c_0[1+(1+c_2)^{1/2}]} - \frac{2c_0[1+(1+c_2)^{1/2}]}{c_0^2 + (x-ct)^2}. \tag{2.5}$$

With the phase speed $c = 0$, (2.4) and (2.5) provide a steady solution.

Property 3. Let the forcing $f(t,x)$ be expressed through the Hilbert integral (1.7) of $\partial^2 y_{\mathrm{w}}/\partial x^2$, where $y_{\mathrm{w}}(t,x)$ stands for the local roughness shape. On the assumption that a solution vanishes sufficiently fast as $x \to \mp\infty$, a relation

$$\frac{\mathrm{d}M}{\mathrm{d}t} = -\int_{-\infty}^{\infty} \mathrm{d}x \int_{-\infty}^{\infty} \frac{\partial^2 y_{\mathrm{w}}/\partial X^2}{X-x}\,\mathrm{d}X, \quad M = \int_{-\infty}^{\infty} A_{\mathrm{w}}\,\mathrm{d}x \tag{2.6}$$

holds, which implies that the conservation law $M = M_0 = \text{const.}$ for the corresponding homogeneous equation. Note that the 'mass' of a soliton propagating against a zero background ($c + c_0^{-1} = 0$) in the absence of forcing ($c_1 = c_2 = 0$) is $M = 4\pi$, i.e. is independent of its amplitude and phase speed (Benjamin 1967).

Property 4. It is known that the homogeneous BDA equation is invariant against a group of affine transformations $t \to \beta^2 t$, $x \to \beta x$, $\tilde{A} \to \beta^{-1}\tilde{A}$. In what follows, the forcing is specified as $y_{\mathrm{w}} = \sigma g(t/t_0)h(x/b)$ with a time-dependent multiplier $g = 0$ if $t \leqslant 0$. As for positive t, we assume g to be a monotonically increasing function on the interval $0 < t < t_0$ becoming $g = 1$ with $t \geqslant t_0$. Applying the same affine transformation, where $\beta = b$, to (1.6) and (1.7) yields

$$\frac{\partial A_{\mathrm{w}}}{\partial t} + A_{\mathrm{w}}\frac{\partial A_{\mathrm{w}}}{\partial x} = \frac{1}{\pi}\int_{-\infty}^{\infty} \frac{\partial^2 A_{\mathrm{w}}/\partial X^2}{X-x}\,\mathrm{d}X - \frac{Q}{\pi} g\left(\frac{t}{T_0}\right)\int_{-\infty}^{\infty} \frac{\mathrm{d}^2 h/\mathrm{d}X^2}{X-x}\,\mathrm{d}X. \tag{2.7}$$

The two similarity parameters $Q = \sigma b$ and $T_0 = t_0/b^2$, appearing here in place of the original three parameters σ, t_0 and b, define the similarity law for all t and x. However, at any sufficiently large moment $t \gg T_0$, the perturbed motion must become effectively independent of the second parameter T_0, owing to the fact that $g = 1$, according to our assumption. Thus, the only similarity parameter Q turns out to be responsible for characteristic features of the oscillation pattern at later stages after switching on the disturbance source.

3. Flow-field bifurcation at $3.92 < Q = Q_1^* < 3.93$

In all computations carried out so far, the function g was simply put equal to t/t_0 (in original variables). So, both upstream- and downstream-propagating waves evolved from the initial data $A_{\mathrm{w}} = 0$. The pseudo-spectral method of Burggraf & Duck (1982), based on applying a fast Fourier transform in x to the forced BDA equation, appears to be pertinent for solving it numerically. An attempt in Zhuk

& Popov (1989) to evaluate solutions using a finite-difference scheme was apparently not successful. Another version (due to Fornberg & Whitham (1978)) of the pseudo-spectral method has been utilized by Mitsudera & Grimshaw (1991) in their computation of internal gravity waves. The shape of a local roughness (again in original variables) was prescribed as $h = \sigma \cos^2 \pi x/b$, $-b < x < b$, whereas $g = 0$ for both $x \leqslant -b$ and $x \geqslant b$. Computationally, it proved to be convenient to take $t_0 = 1$ and $b = 3.5$. Within these limitations, an extensive study has been carried out for a broad range of the similarity parameter Q taking on both positive and negative signs. However, being pressed for space, we concentrate below on discussing the wave generation by humps with $Q > 0$; results for dents specified by $Q < 0$ will be reported elsewhere. As mentioned in the introduction, wave systems generated by dents do not reveal bifurcations and are similar for all Q.

Special care was taken in estimating the error involved in the calculations set forth below. The step size Δx in x and a number N of Fourier modes in the spectral space proved to be highly dependent on a typical magnitude of Q; they were halved and doubled, respectively, until the accuracy of the final results was confirmed. In some runs, Δx was held as low as 0.01 and N reached a value of 2^{14}. However, these extremes entailed an enormous increase in CPU time. Another way to provide a check upon the accuracy of the computation was to compare the oscillatory distributions of A, evaluated numerically at large distances downstream of an obstacle, with oscillatory distributions ensuing from linear analysis. A version of the pseudo-spectral method used turned out to be well suited for minimizing a difference between the two approaches in question. However, only central parts of spatial distributions of A at fixed values of time are presented below, as our main concern is with nonlinear properties of the wave-generation process.

In order to illuminate the statement that the value of a parameter $Q = \sigma b$ defines the disturbance-pattern features, let us trace how strong they change when Q is varying in a narrow interval ($3.92 \leqslant Q \leqslant 3.93$) that contains a threshold value $Q = Q_1^*$. The very existence of Q_1^* can be easily established from a consideration of the mass $M^- = M^-(t)$ transported by a wave system upstream of the obstacle ($-\infty < x \leqslant -3.5$). As seen from the plot of $M^-/4\pi$ presented in figure 1, a solution for $Q = 3.92$ inherent in the subcritical regime I with $Q < Q_1^*$ suffers stability loss if the controlling similarity parameter increases by only 0.01 and becomes $Q = 3.93$. Obviously, a new solution arising from bifurcation must be endowed with completely different properties, this solution is typical of the supercritical regime II specified by $Q > Q_1^*$. According to computed results, bifurcation takes place at an instant $t = t_1^* \approx 150$ (referred to as the incipient transition time) when $M^-(t_1^*) \approx 4\pi$. So, at $t = t_1^*$ the mass of disturbances advancing upstream of the local roughness is approximately equal to the mass of the algebraic soliton (Benjamin 1967).

The flow field development in the subcritical regime I at the threshold of bifurcation can be elucidated by putting $Q = 3.92$. The distribution of the instantaneous displacement thickness $A = y_w - A_w$ over x at $t = 600$ for this case is shown in figure 2, where the first solitary-like wave propagating upstream appears in the well-shaped form, whereas the second is generated just in the vicinity of the disturbing source. The amplitude of the leading solitary wave is approximately twice as large as the disturbance size immediately above the roughness. The way in which A varies in this region is crucial for the overall process of the solitary-wave emission. As shown in figure 3, $A_0(t) = A(t, 0)$ drastically drops shortly after triggering the external agency and then gradually changes around $A_0(t) \approx 0.5$ that can be roughly regarded as a

PHILOSOPHICAL TRANSACTIONS OF THE ROYAL SOCIETY A MATHEMATICAL, PHYSICAL & ENGINEERING SCIENCES

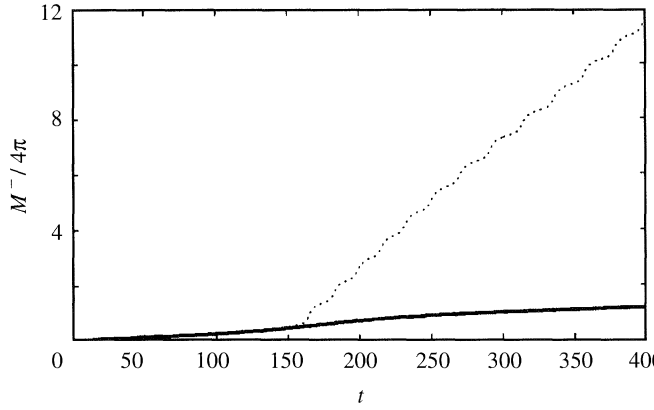

Figure 1. The mass M^- transported by the wave system upstream of the hump as a function of time t: —, $Q = 3.92$; $\cdots$, 3.93.

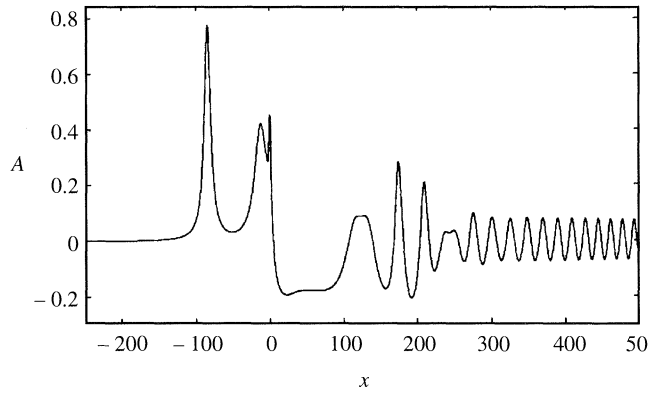

Figure 2. A distribution of the displacement thickness A over distance x in the subcritical regime I: $Q = 3.92$, $t = 600$.

mean value. The slack run of $A_0(t)$, with smooth variations confined to a very narrow band, is at the heart of a large period $T \approx 200$ of solitary-like wave radiation. These waves are of moderate amplitude and move slowly against the oncoming stream; they play an important part in atmospheric phenomena (Mitsudera & Grimshaw 1991).

On the contrary, the wave system downstream of a local uneveness is of primary concern in boundary-layer study. As distinguished from the region located upstream, the disturbance field here begins with a long oscillatory 'tongue' of small amplitude which terminates in solitary-like waves. The short distance between the oscillatory motion and the solitary waves is occupied by weak pulsations of a transitional type. The disturbance system as a whole is separated from the roughness by a depression containing smooth variations of $A(t, x)$ which slowly spreads downstream. The depression area serves as a background for solitary waves to gradually evolve from the last cycles bringing up the rear of the modulated oscillatory tongue. As seen from (2.4) and (2.5) with $c_1 = c_2 = 0$, the algebraic solitons by Benjamin (1967) can travel in the direction of the oncoming stream only against a negative background. If the background becomes zero, the phase speed $c = -c_0^{-1} < 0$; in this case solitons propagate upstream. Thus, formation of the depression area serves as an important condition for solitary-like waves to arise at the tail-end of the modulated oscillatory

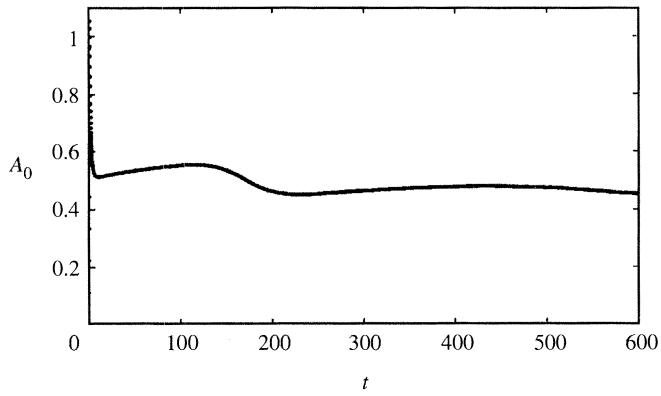

Figure 3. The displacement thickness A_0 at the centre of the hump as a function of time t in the subcritical regime I: $Q = 3.92$.

motion. As inferred from figure 2, solitary waves travelling in the opposite directions (upstream and downstream) emerge in pairs, albeit the time and place of their birth are hardly defined owing to the long period of this process.

When the value of the similarity parameter increases above $Q = Q_1^*$, the flow field changes drastically. However, it is advisable to choose $Q = 5.5$, for example, rather than put $Q = 3.93$, with the objective of eliminating the long evolution inherent in the subcritical regime I during the incipient transition time t_1^*. With $Q = 5.5$, the first solitary-like wave is emitted upstream at $t \approx 20$ (cf. $t_1^* \approx 150$ if $Q = 3.93$). An overall picture of oscillations developed by $t = 50$ with this particular value of $Q = 5.5$ is shown in figure 4. As it might seem at a glance, the disturbance pattern closely resembles that presented in figure 2, except for much larger values of $A(t, x)$. There are solitary waves upstream of the roughness, whereas a more complicated system downstream consists of a small-amplitude oscillatory tongue, a short zone of transitional-type pulsations and solitary waves evolved in the course of the transitional process. A depression region with smooth variations of $A(t, x)$ behind the obstacle again serves as a background allowing solitary waves to be formed from the tail-end cycles of the modulated oscillatory motion. One more function of the depression is to compensate for the mass radiated upstream.

Nevertheless, there exists a crucial distinction between the two regimes in question, which manifests itself primarily in the behaviour of disturbances immediately over the hump ($-3.5 \leqslant x \leqslant 3.5$). In order to shed light on the mechanism behind the fast solitary-wave production in the supercritical regime II, let us turn again to the plot of $A_0(t)$. As figure 5 exhibits, the slack run of this curve when $Q = 3.92$ gives way to vigorous peaky-type pulsations of a nearly constant period $T \approx 18$ for $Q = 5.5$. As a result, the amplitude of the leading solitary wave advancing upstream drops to less than half as low as the size of each peak. However, this amplitude exceeds the amplitude of an analogous solitary-like wave in figure 2 by a factor of about four. In keeping with an increase in size, the propagation speed of solitary waves in the supercritical regime II also gets enhanced several times, so that they are capable of moving fast enough against the oncoming stream. The same statement holds true with regard to the solitary-like waves sweeping downstream at the rear of the modulated oscillatory tongue; their amplitude, reckoned from the depression level, proves to be of the same order as the amplitude of disturbances ahead of the local roughness. One more feature is recognizible and worthy of note in the run of

PHILOSOPHICAL TRANSACTIONS OF THE ROYAL SOCIETY A MATHEMATICAL, PHYSICAL & ENGINEERING SCIENCES

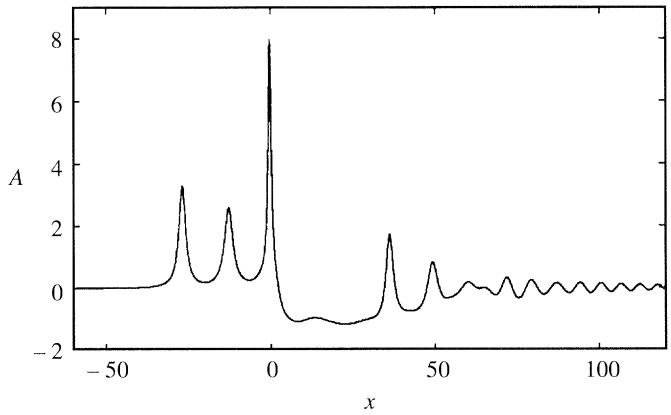

Figure 4. A distribution of the displacement thickness A over distance x in the supercritical regime II: $Q = 5.5$, $t = 50$.

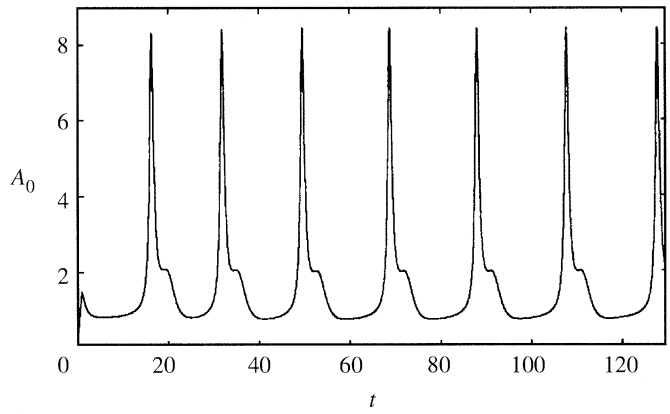

Figure 5. The displacement thickness A_0 at the centre of the hump as a function of time t in the supercritical regime II: $Q = 5.5$.

a curve in figure 5: a sharp drop of $A_0(t)$ within each oscillation cycle experiences a small kink before reaching the minimum value.

To further illustrate fundamental properties of the nearly periodic process in the vicinity of the hump, figure 6 provides its phase portrait in a plane $(A_0, \dot{A}_0 = \mathrm{d}A_0/\mathrm{d}t)$ for values 5.5, and 7.5 of the similarity parameter Q. In all three cases, we have a region in the form of a narrow closed strip filled by oscillation coils. This loop-shaped region rapidly stretches as Q grows, giving rise to the second tiny loop in its lower part, not far from the origin. The cause for the lesser loop to gradually emerge is directly related to evolution of a kink in $A_0(t)$ mentioned above. With Q fixed, the oscillation process bears similarities to a limit cycle, but departs from this since the frequencies associated with coils inside any one of the narrow bands in figure 6 are slightly varying. On the other hand, the BDA equation belongs to dynamical systems of Hamiltonian form (Case 1980). As such, it cannot exhibit limit cycles, defined in the strict sense, among attracting sets.

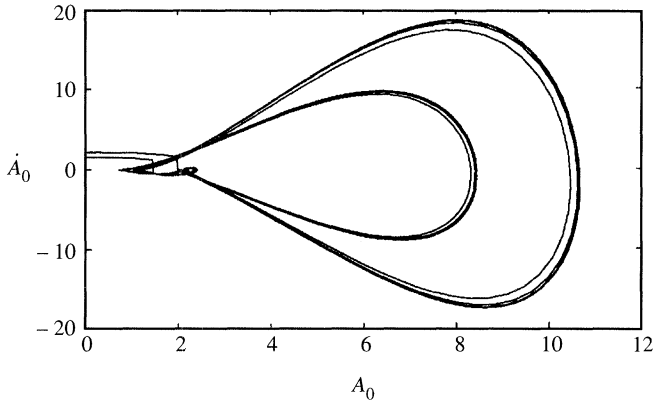

Figure 6. The phase portrait of oscillations at the centre of the hump in the plane $(A_0, \dot{A}_0)$ for $Q = 5.5$ and 7.5.

4. Gradual evolution of disturbance pattern

The flow field undergoes a smooth evolution when the similarity parameter Q grows step by step in the range $Q_1^* < Q < Q_2^*$, the latter being a value defining the next bifurcation. According to computed results (see below), Q_2^* is fixed by inequalities $51.48 < Q_2^* < 51.49$. Owing to space limitations, we skip any in-depth discussion of the wave-system properties as a function of x at different t. The only point to be nevertheless mentioned is that the solitary-wave train upstream of a hump creates an inherent positive background clearly discernible even at the initial stage in figure 4. This background is, by no means, uniform and the amplitudes of solitary-like waves are equal, as might be inferred from Zhuk & Popov (1989), where the emission of BDA solitary waves upstream of an obstacle was probably first reported. An extensive study of this phenomenon for the range of Q under discussion can be found in Mitsudera & Grimshaw (1991).

The key element of gradual evolution when $Q_1^* < Q < Q_2^*$ comes from alterations occuring in the form of vigorous pulsations immediately over the hump. As before, the process is best characterized by a plot of $A_0(t)$ given in figure 7 for $Q = 51.48$. From a comparison between figures 5 and 7, we observe that a peak surmounting each oscillation cycle with $Q = 5.5$ becomes of larger size and much more clear cut when Q amounts to 51.48. A nearly constant period of oscillations shortens from $T \approx 18$ to $T \approx 3.2$, respectively. A small kink on the leeward slope of a peak in figure 5 transforms into a spike within the same cycle in figure 7. This spike is situated just in the middle of two main neighbouring peaks. The role of the spike is crucial for the subsequent bifurcation to occur. Each oscillation cycle gives rise to a solitary wave, carrying the mass $M_{\mathrm{SW}}^- \approx 4\pi$ in the region upstream of the hump. Simultaneously, a gently sloping disturbance with $M^+ \approx -4\pi$ is brought into the depression zone extending downstream.

Figure 8 gives the phase portrait of the nearly periodic process using coordinates A_0 and $\dot{A}_0$. As in figure 6, the process is mapped onto a region in the form of a narrow strip filled by oscillation coils. However, there is an important distinction between the two types of phase-plane portraits since small spikes, alternating with the main peaks in the distribution of $A(t, x)$ for $\Delta = 51.48$, result in another extremely thin band imbedded in the primary larger-sized loop. The origin of the band is clearly recognizable in a tiny loop emerging and slowly developing in the phase-plane portraits, illustrated by figure 6. As a consequence, a double-loop-shaped region serves

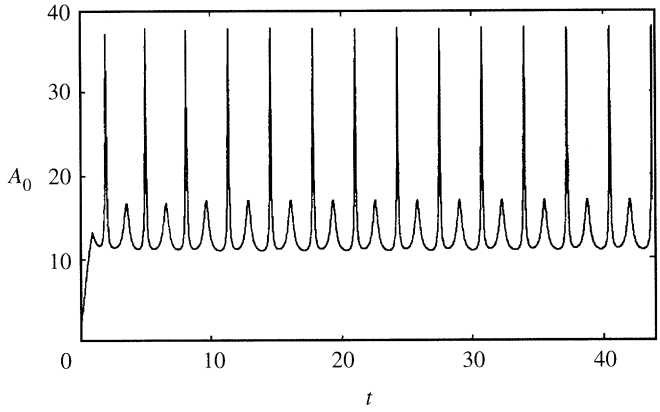

Figure 7. The displacement thickness A_0 at the centre of the hump as a function of time t in the subcritical regime III: $Q = 51.48$.

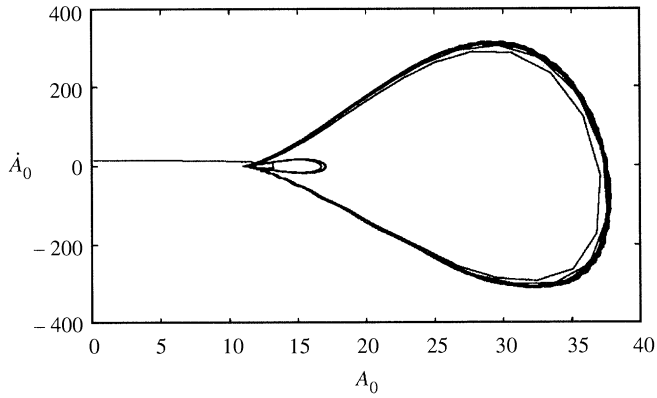

Figure 8. The phase portrait of oscillations at the centre of the hump in the plane $(A_0, \dot{A}_0)$ for $Q = 51.48$.

as an image of the vigorous pulsation process at the threshold of the next bifurcation, when the supercritical regime II turns to subcritical regime III. In keeping with Smith (1988), peaky-type disturbances in boundary-layer flows can eventually terminate in the near-wall tier eruption. Therefore, evolution of the oscillation cycle at the hump crest towards sharpening variations of A, with Q growing, is highly conducive to the breakdown of laminar motion and accelerates the onset of transition.

5. Flow-field bifurcation at $51.48 < Q = Q_2^* < 51.49$

In order to reveal this bifurcation in the simplest way, let us consider once more the mass $M^- = M^-(t)$, transported by the wave system in the region $-\infty < x \leqslant -3.5$ upstream of the obstacle. Figure 9 attests to a sudden jump in the mass-production rate if the controlling similarity parameter $Q = 51.48$, characteristic of the subcritical regime III, increases by 0.01 and becomes $Q = 51.49$. This change can be attributed to the supercritical regime IV coming in place of the subcritical regime III at the incipient transition time $t_2^* \approx 11$. The value t_2^* is made up of a period $t_0 = 1$ of triggering the disturbing source and a span of about three cycles of the subcritical regime III which persists until bifurcation. Hence, we have, $M^-(t_2^*) = 3M_{\mathrm{SW}}^- \approx 12\pi$.

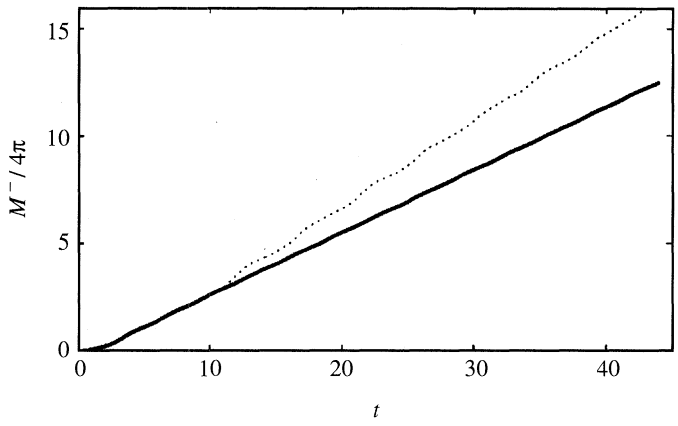

Figure 9. The mass M^- transported by the wave system upstream of the hump as a function of time t: —, $Q = 51.48$; $\cdots$, 51.49.

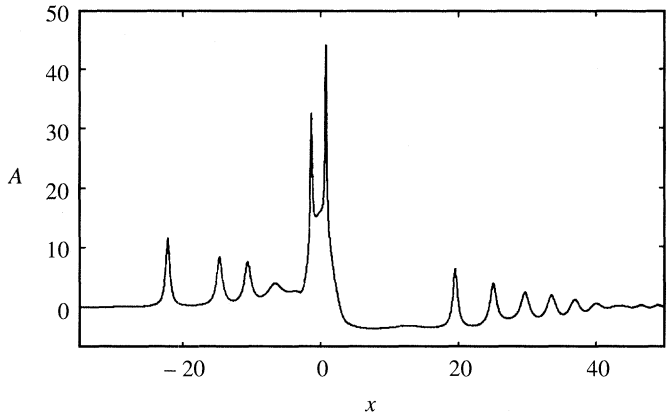

Figure 10. A distribution of the displacement thickness A over distance x in the supercritical regime IV: $Q = 70$, $t = 10$.

Key properties of the supercritical regime IV along with a new mechanism at the heart are set forth below.

We may visualize a more complicated motion in physical space from figure 10 drawn for $Q = 70$ at $t = 10$. The overall wave system generated in this case bears certain similarities to that shown in figure 4, where $Q = 5.5$, and even to the disturbance pattern in figure 2 with $Q = 3.92$. A solitary-wave train is seen to propagate upstream of the hump against an intrinsic positive background, whereas the region on the leeward side involves a modulated oscillatory tongue, a few solitary-like waves arising at its tail-end, as well as a depression area spreading between the last of these waves and the obstacle. Of course, the swing of oscillations is large compared with the typical size in the subcritical regime III, especially immediately over the disturbing source confined to $-3.5 \leqslant x \leqslant 3.5$. However, the basic distinction derives from the nature of disturbance distribution in the wave systems both upstream and downstream of the hump. They seem to be not as well-organized as for lesser values of $Q < Q_2^*$, the double-peaky large-amplitude burst over the hump points to the same conclusion.

The latter is clearly substantiated by inspecting the behaviour of $A_0(t)$ with the

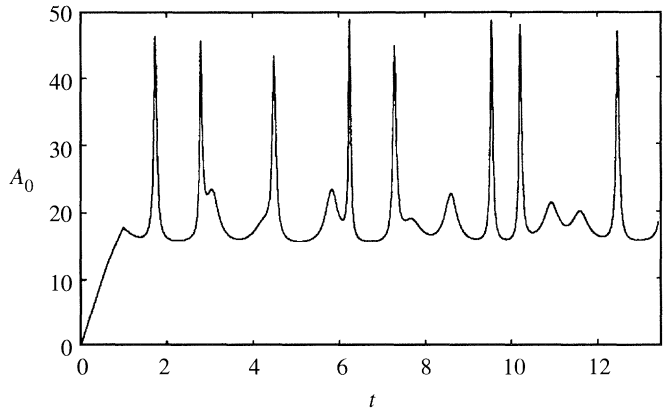

Figure 11. The displacement thickness A_0 at the centre of the hump as a function of time t in the supercritical regime IV: $Q = 70$.

same value $Q = 70$ as t increases. A remarkable alternation of main peaks and spikes, peculiar to figure 7 for $Q = 51.48$, changes, if $Q = 70$, to a distribution in figure 11, where peaks and spikes accompanied by kinks come in an erratic manner rather than being governed by an apparent rule. What is more, the distinctions between spikes and kinks are hardly discernible. The reference time of this aperiodic process reduces roughly to $T \approx 1.5$, compared with a nearly constant period $T \approx 3.2$ of oscillations when $Q = 51.48$. Some further growth in the amplitude of $A_0(t)$ is also observable but does not manifests itself in dramatic form.

On the contrary, the phase portrait of the process in the plane $(A_0, \dot{A}_0)$ is drastically modified; from narrow closed strips in figure 6 specified by $Q = 5.5$ and 7.5 to a wide region in figure 12 drawn for $Q = 70$. Large-sized coils and small loops produced by peaks, spikes and kinks superimpose in a subdomain located near the origin. So, the nearly periodic process over the hump, typical of the subcritical regime III, collapses into irregular pulsations with erratic sequences of amplitudes and characteristic times when passing through a bifurcation value $Q = Q_2^*$. As to the nature of the sequences which feature the supercritical regime IV, no decisive conclusion may be inferred on the basis of the computed results. However, abrupt sharpening variations of A mediates the onset of bursting phenomena (Smith 1988).

6. Randomization onset

The following brief discussion pursues the aim of providing evidence that the onset of random disturbances in the form of 'Hamiltonian chaos' is inherent in the solitary-wave stage of fluid motion. To simplify the problem we address a viscous flow past a plate mounted vertically in the gravity field and heated. The solitary-wave stage of disturbance propagation obeys, in this case, the KdV equation, which was pointed out by Korteweg & de Vries as far back as 1895 in the context of shallow water waves. In keeping with Zhuk & Ryzhov (1982) and Smith & Burggraf (1985), the homogeneous KdV equation is obtainable from (1.1) and (1.2), with p related to A through $p = -\partial^2 \tilde{A}/\partial x^2$, instead of (1.3). Taking advantage of this interaction law, we can extend the analysis presented in the introduction and derive the aforementioned equation with a forcing term $f = \partial^3 y_w/\partial x^3$ coming in place of (1.7) if the shape of an uneven wall is fixed by $y = y_w(t, x)$. For instance, let the wall be flexible

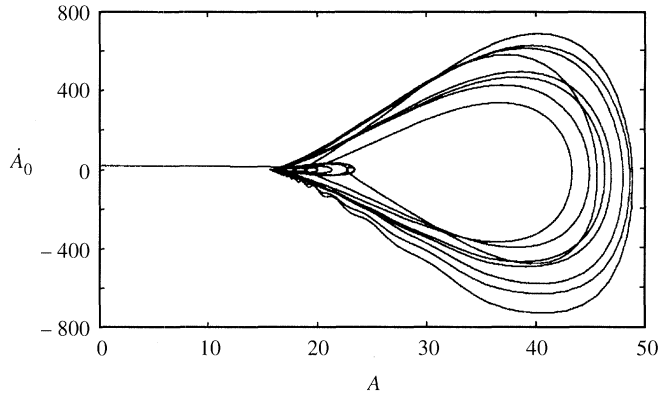

Figure 12. The phase portrait of oscillations at the centre of the hump in the plane $(A_0, \dot{A}_0)$ for $Q = 70$.

and slightly disturbed by a travelling wave sweeping downstream. Then the wavy plate serves as an external agency $f = f(kx - \omega t) = \partial^3 y_w(kx - \omega t)/\partial x^3$ for the fluid motion in a boundary layer adjacent to the solid base. Presumably, the forced KdV equation first appeared in related studies on the flow of a stratified fluid over topography (Grimshaw & Smyth 1986) and surface waves in a shallow water channel (Camassa & Wu 1991*a*, *b*). Note that the simplest way to reproduce and observe the process of solitary or periodic wave interaction with convected forcing is likely to use a water tank as an experimental setup (Davis & Acrivos 1967; Lee *et al.* 1989) leaning upon the mathematical analogy between the boundary-layer and deep/shallow-water nonlinear disturbances.

As we see, physical problems governed by the BDA and KdV equations are very similar in nature; both arise in an attempt to shed more light on an essentially nonlinear stage of wave propagation in boundary-layer flows before transition. From the purely mathematical viewpoint, these integrable evolution equations have many properties in common: multi-periodic and multi-soliton solutions, pole expansions in a complex plain, an infinitely large number of conservation laws, Lax pairs, inverse scattering transforms, etc. For an in-depth discussion see, for example, Ablowitz & Clarkson (1991). On the other hand, dynamical-systems theory is directly applicable to analysing a broad class of solutions to the forced KdV equation insofar as dispersion is expressed in the latter case in terms of the third derivative rather than a Hilbert integral of a desired function. So, information gained from this study can provide useful guidelines for investigating forced oscillations controlled by the inhomogeneous BDA model.

With a forcing term, taken in the form $f = f(kx - \omega t)$, the KdV equation admits a similar travelling-wave-type solution $A_w = F(kx - \omega t)$. On applying the aforementioned affine transformation, F is obtainable from a system of two first-order differential equations

$$\frac{\mathrm{d}F}{\mathrm{d}\xi} = \frac{\partial H}{\partial \dot{F}} = \dot{F}, \quad \frac{\mathrm{d}\dot{F}}{\mathrm{d}\xi} = -\frac{\partial H}{\partial F} = -\omega F + \tfrac{1}{2}F^2 + C + \delta I_w(\xi), \tag{6.1}$$

with $I_w = \sin\xi$, $\xi = x - t$ standing for a harmonic excitation normalized by δ and

$$H = H_0(F, \dot{F}) + \delta H_1(\xi, F) = \tfrac{1}{2}\dot{F}^2 + \tfrac{1}{2}\omega F^2 - \tfrac{1}{6}F^3 - CF - \delta F I_w(\xi) \tag{6.2}$$

being a Hamiltonian function. The model (6.1), (6.2) describes nonlinear oscillations of a pendulum with quadratic stiffness and no friction.

A phase-plane portrait of (6.1), (6.2) with $\delta = 0$ includes a centre $C : F_c = \omega - (\omega^2 - 2C)^{1/2}$, $\dot{F}_c = 0$ surrounded by a nested family of closed orbits, and a saddle $S : F_s = \omega + (\omega^2 - 2C)^{1/2}$, $\dot{F}_s = 0$ with an alpha-shaped separatrix loop passing through it. It is remarkable that the loop is an image of the KdV soliton (Drazin & Johnson 1989)

$$F_{\mathrm{sol}} = F_s - \frac{3(\omega^2 - 2C)^{1/2}}{\mathrm{ch}^2\,\eta}, \quad \dot{F}_{\mathrm{sol}} = \frac{3(\omega^2 - 2C)^{3/4}\,\mathrm{sh}\,\eta}{\mathrm{ch}^3\,\eta}, \quad \eta = \frac{(\omega^2 - 2C)^{1/4}\xi}{2}, \tag{6.3}$$

which moves downstream against the positive background $F = F_s > 0$. The separatrix loop may be considered as the base of a cylindrical surface with generators parallel to the ξ-axis in the three-dimensional phase space. When $\delta \neq 0$, this surface splits into the stable $W_s(\delta)$ and unstable $W_u(\delta)$ manifolds, the relative locations of which control the dynamics of the system (6.1), (6.2). A Mel'nikov function, which measures the distance between $W_s(\delta)$ and $W_u(\delta)$, is defined by (Guckenheimer & Holmes 1983)

$$J(\varphi_0) = \int_{-\infty}^{\infty} \left\{ H_0[F_{\mathrm{sol}}(\xi), \dot{F}_{\mathrm{sol}}(\xi)], H_1 \left[\xi + \frac{\varphi_0}{\omega}, F_{\mathrm{sol}}(\xi) \right] \right\} \mathrm{d}\xi, \tag{6.4}$$

where the braces denote canonical Poisson brackets. Perturbation calculations in (6.4) are supposed to rely on the initial soliton solution (6.3). Taking advantage of expressions for both $H_0(F, \dot{F})$ and $H_1(\xi, F)$ ensuing from (6.2), yields (Burov & Ryzhov 1992)

$$J(\varphi_0) = 12\pi\,\mathrm{sh}\,\pi(\omega^2 - 2C)^{-1/4}[\mathrm{ch}\,2\pi(\omega^2 - 2C)^{-1/4} - 1]^{-1} \cos\varphi_0. \tag{6.5}$$

Thus, the Mel'nikov function possesses an infinite set of simple zeros $\varphi_0 = (n + \frac{1}{2})\pi$, $n = \ldots, -1, 0, 1, \ldots$ with a consequence that $W_s(\delta)$ and $W_u(\delta)$ intersect indefinitely many times. This fact is embodied in a Poincaré map illustrated by figure 13, where the homoclinic tangle contains a wide variety of different trajectories. They determine the complex dynamics of the Hamiltonian system (6.1), (6.2) in spite of its apparent simplicity.

A far more gentle analysis is needed when considering the splitting of closed periodic orbits around the centre C in the phase plane $(F, \dot{F})$ in response to a periodic forcing. The vanishing of the Mel'nikov function along an orbit, such that the corresponding free-oscillation frequency is rationally commensurable with the forcing frequency, points to the existence of a subharmonic resonance. The presence of the homoclinic tangle here leads to complex dynamics within a subharmonic resonance band. A 'beyond all orders', or exponentially small version, of the Mel'nikov function has been recently shown by Scheurle *et al.* (1992) to provide a legitimite mathematical tool for justifying the existence of the homoclinic tangle associated with a subharmonic resonance. The Poincaré map in figure 13 gives a good idea of the homoclinic tangle close to a periodic orbit.

The conclusion of conceptual importance from a complete analysis of trajectories within the homoclinic tangles of both types is with regard to the development of dynamics referring to as Hamiltonian chaos, which is, meanwhile, not a strange attractor (Guckenheimer & Holmes 1983). The behaviour of the orbits in question is random. The last statement can be reformulated in terms of the original problem on disturbances propagating through a heated jet adjacent to a vibrating plate. As soon as they enter an essentially nonlinear stage, large-sized well-organized structures would be expected to emerge in the form of solitary waves. Really, as was argued in

PHILOSOPHICAL TRANSACTIONS OF THE ROYAL SOCIETY A MATHEMATICAL, PHYSICAL & ENGINEERING SCIENCES

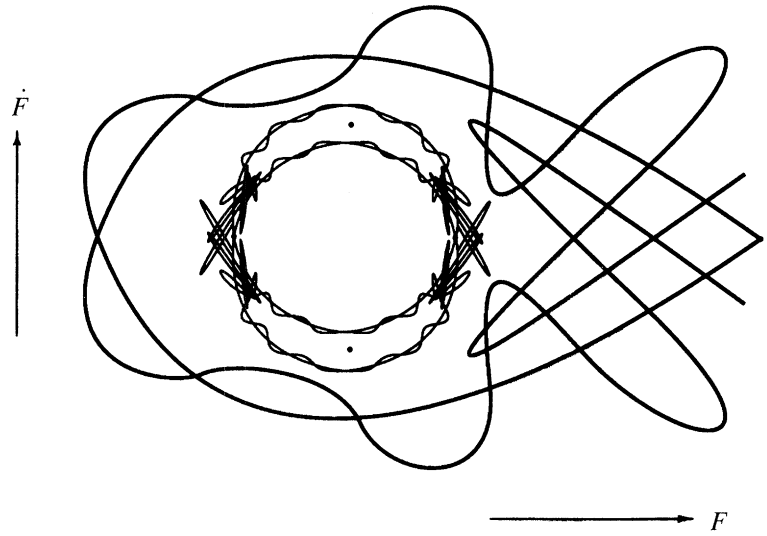

Figure 13. The Poincaré map with two homoclinic tangles emerging from the splitting of the alpha-shaped separatrix and a subharmonic periodic orbit.

the introduction with reference to experimental data from Kachanov *et al.* (1993), this is the case as applied to a Blasium boundary layer where the sharp narrow spike embedded in each oscillation cycle of a nonlinear TS wave train is endowed with soliton properties. Therefore, the breakdown of the high-amplitude disturbance pattern under the influence of a vibrating plate should be accompanied by the generation of various more complex forms of motion and, in particular, random pulsations. Thus, the role played by high-amplitude solitary and periodic waves is twofold: they make up large coherent structures and, at the same time, can provoke chaotic pulsations (Ryzhov 1991; Burov & Ryzhov 1992). Both properties of the nonlinear phenomenon are interconnected and inseparable. Certainly, the above conclusion calls for careful verification in wind-tunnel tests.

The authors would like to express their sincere gratitude to Professor J. D. Cole for encouraging discussions and comments which led, in particular, to the formulation of the similarity law. Special thanks are due to Professor G. Kovačič for attracting the authors' attention to a phenomenon of the exponentially small splitting of separatrices. The helpful criticism of the 'Brown Bag Seminar' (Rensselaer Polytechnic Institute) participants is also recognized. The study has been carried out with the support to E.V.B.-R. of NAS under CAST grants and to O.S.R. of AFOSR under grant F49620-93-1-002LDEF.

References

Ablowitz, M. J. & Clarkson, P. A. 1991 *Solitons, nonlinear evolution equations and inverse scattering.* Cambridge University Press.

Benjamin, T. B. 1967 Internal waves of permanent form in fluids of great depth. *J. Fluid Mech.* **29**, 559–592.

Burggraf, O. R. & Duck, P. W. 1982 Spectral computation of triple-deck flows. In *Proc. Symp. on Numerical and Physical Aspects of Aerodynamic flow* (ed. T. Cebeci), pp. 145–158. Berlin: Springer.

Burov, A. A. & Ryzhov, O. S. 1992 The onset of stochastic pulsations at the earlier nonlinear stage of disturbance development in an incompressible near-wall jet. *Prikl. Math. Mekh.* **56**, 1016–1022 (Engl. transl. 1992 *J. appl. Math. Mech.* **56**, 921–927).

Camassa R. & Wu, T. Y. 1991*a* Stability of forced steady solitary waves. *Phil. Trans. R. Soc. Lond.* A **337**, 429–466.

Camassa, R. & Wu, T. Y. 1991*b* Stability of some stationary solutions for the forced KdV equation. *Physica* **51D**, 295–307.

Case, K. M. 1980 The Benjamin-Ono equation: a remarkable dynamical system. *Ann. Nucl. Energy* **7**, 273–277.

Craik, A. D. D. 1971 Nonlinear resonant instability in boundary layers. *J. Fluid Mech.* **50**, 393–413.

Davis, R. E. & Acrivos, A. 1967 Solitary internal waves in deep water. *J. Fluid Mech.* **29**, 593–607.

Drazin, R. G. & Johnson R. S. 1989 *Solitons: an introduction*. Cambridge University Press.

Fornberg, B. & Whitham, G. B. 1978 A numerical and theoretical study of certain nonlinear phenomena. *Phil. Trans. R. Soc. Lond.* A **289**, 373–404.

Grimshaw, R. H. J. & Smyth, N. 1986 Resonant flow of a stratified fluid over topography. *J. Fluid Mech.* **169**, 429–464.

Guckenheimer, J. & Holmes, P. J. 1983 *Nonlinear oscillations, dynamical systems, and bifurcations of vector fields*. Berlin: Springer.

Kachanov, Y. S., Kozlov, V. V. & Levchenko, V. Y. 1977 Nonlinear development of a wave in a boundary layer. *Izv. Akad. Nauk SSSR, Mekh. Zhidk. Gaza* **3**, 49–58 (Engl. transl. 1977 *Fluid Dyn.* **12**, 383–390).

Kachanov, Y. S., Kozlov, V. V., Levchenko, V. Y. & Ramazanov, M. P. 1989 The nature of K-breakdown of laminar boundary layer. *Izv. Sibirsk. Otd. Akad. Nauk SSSR, Ser. Tekh. Nauk* **2**, 124–158 (in Russian).

Kachanov, Y. S., Ryzhov, O. S. & Smith, F. T. 1993 Formation of solitons in transitional boundary layers: theory and experiment. *J. Fluid Mech.* **191**, 273–297.

Klebanoff, P. S., Tidstrom, K. D. & Sargent, L. M. 1962 The three-dimensional nature of boundary-layer instability. *J. Fluid Mech.* **12**, 1–34.

Korteweg, D. J. & de Vries, G. 1895 On the change of form of long waves advancing in a rectangular canal and a new type of long stationary waves. *Phil. Mag.* **39**, 422–443.

Landau, L. D. & Lifshitz, E. M. 1944 Mechanics of continua. Moskwa: Gostekhizdat (Engl. transl. 1959 *Fluid mechanics*. London: Pergamon).

Lee, S. J., Yates, G. T. & Wu, T. Y. 1989 Experiments and analysis of upstream-advancing solitary waves generated by moving disturbances. *J. Fluid Mech.* **199**, 569–593.

Mitsudera, H. & Grimshaw, R. 1991 Effects of radiative damping on resonantly generated internal gravity waves. *Stud. appl. Math.* **84**, 183–206.

Ryzhov, O. S. 1991 Boundary-layer stability and paths to transition: theoretical concepts and experimental evidence. In *1st European Fluid Mechanics Conf., Cambridge, UK.*

Scheurle, J., Marsden, J. E. & Holmes, P. 1992 Exponentially small estimates for separatrix splitting. (Submitted).

Smith, F. T. 1988 Finite-time break-up can occur in any unsteady interactive boundary layer. *Mathematika* **35**, 256–273.

Smith, F. T. & Burgraf, O. R. 1985 On the development of large-sized short-scaled disturbances in boundary layer. *Proc. R. Soc. Lond.* A **399**, 25–55.

Stuart, J. T. 1960 On the nonlinear mechanics of wave disturbances in stable and unstable parallel flows. Part 1. The basic behaviour in Plane Poiseuille flow. *J. Fluid Mech.* **9**, 353–370.

Zhuk, V. I. & Popov, S. P. 1989 On the solutions of the inhomogeneous Benjamin-Ono equations. *Zh. vych. Mat. mat. Fiz.* **29**, 1852–1862 (Engl. transl. 1989 *U.S.S.R. Comput. Math. Math. Phys.* **29**, 176–183).

Zhuk, V. I. & Ryzhov, O. S. 1982 Locally inviscid perturbations in a boundary layer with self-induced pressure. *Dokl. Akad. Nauk SSSR* **263**, 56–59 (Engl. transl. 1982 *Soviet Phys. Dokl.* **27**, 177–179).

PHILOSOPHICAL TRANSACTIONS OF THE ROYAL SOCIETY A MATHEMATICAL, PHYSICAL & ENGINEERING SCIENCES